Dose-dependent toxicity of fluorescein isothiocyanate-labeled zeolitic imidazolate framework-8 nanoparticles in Swiss albino mice

Arun Unnikrishna Pillai[1], Sreeja Rajeswari[2], and Annie Abraham[3]*

ABSTRACT

Nanoscale metal–organic frameworks have attracted significant attention from the research community due to their tailorable composition and structures, high porosity, and facile surface modification. The development of targeted nanoscale drug delivery systems (DDSs) is important in improving target specificity, reducing side effects, and enhancing the therapeutic efficacy of drugs. At the same time, toxicological studies are crucial in the development and safe use of novel DDSs to eliminate unforeseen health risks. Such analyses investigate nano-biointeractions and evaluate potential cytotoxic, genotoxic, or immunotoxic effects. In this study, we synthesized nano-sized luminescent fluorescein 5-isothiocyanate (FITC)-labeled zeolitic imidazolate framework-8 (ZIF-8) nanoparticles through a simple chemical approach. Basic characterization studies of the nanoparticles were performed using X-ray diffraction, scanning electron microscopy (SEM), transmission electron microscopy (TEM), and photoluminescence (PL) analysis. SEM and TEM analysis confirmed the dodecahedral shape of the nanoparticles with an average size of 65–70 nm. The fluorescent emission from FITC-labeled ZIF-8 nanoparticles corresponded to the typical emission of incorporated FITC in the ZIF-8. The PL emission spectrum confirmed the incorporation of FITC into the ZIF-8, thereby offering fluorescence probing of the nanoparticles. In addition, we investigated the *in vivo* toxicity profile of FITC-labeled ZIF-8 nanoparticles in 6–8-week-old Swiss albino mice to establish safe dosage limits. The results of hematological, biochemical, inflammatory, antioxidant, and immunotoxicity markers, as well as histopathological evaluation, showed no significant toxicity at moderate doses of FITC-labeled ZIF-8 nanoparticles. Thus, FITC-labeled ZIF-8 nanoparticles can be safely employed as a suitable drug delivery platform for *in vivo* applications, such as in cancer therapy.

Keywords:
Zeolitic imidazolate framework-8; Metal–organic frameworks; *In vivo* studies; Mouse; Toxicity

***Corresponding author:**
Annie Abraham,
annieab@keralauniversity.ac.in

How to cite this article:
Pillai AU, Rajeswari S, Abraham A. Dose-dependent toxicity of fluorescein isothiocyanate-labeled zeolitic imidazolate framework-8 nanoparticles in Swiss albino mice. *Biomater Transl.* **2025**

doi: 10.12336/bmt.25.00054

1. Introduction

The emergence of nano-based drug delivery systems (DDSs) marks a significant advancement in pharmaceutical science and medicine. Nanotoxicology is a novel and growing research area that studies the toxicological profiles of nanomaterials in living organisms. It explores the physicochemical and biological properties of nanomaterials, as well as the alterations caused by these materials within organisms and their mechanisms of action. Assessment of toxicity is a crucial step in the development of new drugs for clinical applications. It bridges the gap between innovation and responsible clinical translation, ensuring that these DDSs are both effective and safe for human use. Toxicological studies before the administration of potential new drugs occupy a significant part of the non-clinical tests recommended by the regulatory agencies. Among the two broad categories of toxicity evaluations (*in vitro* and *in vivo* studies), *in vivo* studies occupy the most relevant position as they investigate the adverse effects of chemicals

within an intact, living organism, such as a laboratory animal. Generally, *in vivo* studies provide adequate and reliable data to comprehend the absorption, distribution, metabolism, and excretion of nanomaterials. *In vivo* studies are irreplaceable as variations in biological responses of nanoparticles invalidate the extrapolation of *in vitro* study results. Toxicological studies help identify the potential side effects of newly developed drugs as they can be detrimental to the immune system, genome integrity, and key organ functionalities. Species-, organ-, and dose-specific toxicity of the new drugs are identified through preclinical toxicity testing on different biological systems[1,] and the levels of toxicity are investigated through quantitative and statistical analysis.

Toxicological evaluations can be performed using different toxicological assays, which strictly adhere to Good Laboratory Practices. Toxicity assays measure the relationship between the dose of the administered drug and the potential toxic responses in different organs of laboratory animals. The design of the study and the selection of the experimental protocol must provide sufficient information to evaluate the risks and safety of the new drug. Toxicological studies also evaluate the accumulation of the administered material in a specific organ or tissue. The toxicity of nanoparticles in *in vivo* systems can be determined through acute and sub-acute toxicity evaluations. Sub-acute toxicity evaluation can be conducted for a period of 14 or 28 consecutive days with daily administration of the test compound through intraperitoneal (IP) or intravenous routes in rodents.[2]

DDSs based on metal–organic frameworks (MOFs) have gained significant attention in recent years due to their high surface area, tunable porosity, potential for functionalization, and stimuli-responsive behavior. MOFs are composed of metal ions or clusters coordinated to organic ligands, forming porous crystalline structures. These properties make them ideal candidates for controlled, targeted, and efficient drug delivery. Zeolitic imidazolate framework-8 (ZIF-8) is a type of MOF composed of zinc ions and 2-methylimidazolate linkers. It is particularly notable for its high porosity, thermal stability, and pH-sensitive degradability, making it a promising candidate for drug delivery, biosensing, and therapeutic applications. ZIF-8 is pH-sensitive and degrades under acidic conditions, such as the tumor microenvironment or inside lysosomes. This makes it ideal for the targeted release of therapeutics. Paclitaxel-loaded ZIF-8 nanoparticles have been reported for their promising potential in prostate cancer treatment.[3] ZIF-8 has been demonstrated to be a promising carrier for pH-responsive controlled drug release and for achieving high drug loading of doxorubicin (DOX).[4] *In vitro* imaging in HeLa and A549 cells confirmed high uptake and enhanced contrast, validating the use of fluorescently labeled ZIF-8 nanoparticles in bio-imaging applications. ZIF-8 has been extensively studied *in vivo* for its potential in drug delivery, imaging, and cancer therapy. BALB/c mice with subcutaneous tumors were injected intravenously with 6-carbofluorescein-labeled iron (II, III) oxide encapsulated in ZIF-8.[5] A multifunctional ZIF-8 nanoplatform was developed for the co-delivery of DOX, radiotherapy agents, and targeting ligands for colorectal cancer therapy using C57BL/6 mice bearing HT-29 tumors.[6] The biodistribution and metabolism of manganese-doped ZIF-8 were investigated *in vivo*.[7] MCF-7 tumor-bearing nude mice were used to evaluate the *in vivo* photothermal effect of gold encapsulated in ZIF-8/DOX nanocomplex.[8] The well-defined pores, high pore volume, outstandingly high surface area, superb drug loading capacity, and prominent pH-triggered release behavior make ZIF-8 a perfect drug delivery platform. In this study, the ZIF-8 nanoparticles were labeled with a non-toxic fluorescent dye, fluorescein 5-isothiocyanate (FITC), as luminescent probes, to achieve high sensitivity in tracing the carrier nanoparticles using fluorescence spectroscopy, thereby understanding their behavior during *in vitro* and *in vivo* applications. In addition, we investigated the *in vivo* toxicity profile of FITC-labeled ZIF-8 nanoparticles in 6–8-week-old Swiss albino mice to ensure the safe dosage limit of the nanoparticles. The toxicity profile of the nanoparticles was compared with the widely studied alkylating agent cyclophosphamide (CP), whose toxicological and pharmacological effects are predictable and reproducible in various animal models. The characteristics, including mutagenic and clastogenic properties (causing DNA damage and chromosomal aberrations), inhibition of humoral and cell-mediated immunity (making it a benchmark for testing immunotoxicity), and suppression of bone marrow cell production (affecting the production of blood cells), make CP an ideal positive control for toxicity evaluations. In this study, the *in vivo* toxic effects of different doses of nanoparticles after daily IP injection over 14 consecutive days were evaluated. The results were compared with untreated and CP-treated mouse models.

2. Materials and methods

2.1. Synthesis of fluorescein 5-isothiocyanate-labeled ZIF-8 nanoparticles

The procedure reported by Cravillon *et al.*[9] was employed with slight modifications for nanoparticle synthesis. We used zinc nitrate hexahydrate ($Zn[NO_3]_2{\cdot}6H_2O$) (SRL Zinc Nitrate Hexahydrate extrapure AR, 98%, Sisco Research Laboratories Pvt Ltd, India) as the metal source, 2-methylimidazole (HMIM) (2-Methylimidazole pure, 99%, Sisco Research Laboratories Pvt Ltd, India) as the linker, and high-performance liquid chromatography-grade methanol (Merck Methanol Lab Reagent LR Grade, 99%, Merck India Ltd, India) as the solvent. The $Zn(NO_3)_2{\cdot}6H_2O$ and HMIM solutions in methanol were prepared separately in two clean glass beakers (1.5 g of $Zn[NO_3]_2{\cdot}6H_2O$ and 3.34 g of HMIM in 50 mL of methanol, respectively). Then, 1.5 mL (2.0 mg/mL) of FITC solution

[1]Department of Biochemistry, Faculty of Science, Government College Kariavattom, Thiruvananthapuram, Kerala, India; [2]Department of Physics, Faculty of Science, Mar Ivanios College (Autonomous), Thiruvananthapuram, Kerala, India; [3]Department of Biochemistry, School of Life Sciences, University of Kerala, Thiruvananthapuram, Kerala, India

(Sigma Aldrich, USA) was added slowly to the zinc nitrate solution under vigorous stirring (1,000 rpm) for 5 min. Upon adding the FITC solution, a color change to yellow was observed in the $Zn(NO_3)_2 \cdot 6H_2O$ solution. Subsequently, the HMIM solution was added in a dropwise manner to the $Zn(NO_3)_2 \cdot 6H_2O$ solution under vigorous stirring. After the addition of HMIM, the yellow solution turned milky within 2 min, indicating the formation of ZIF-8 nanoparticles. The stirring process was allowed to proceed for 2 h, and the resulting colloid was centrifuged at 12,000 rpm at 4°C for 30 min (Eppendorf 5804 R, Eppendorf AG, Germany) to obtain a pale-yellow precipitate. The precipitate was washed three times with methanol to remove unreacted reactants and then kept in a thermostatic hot air oven overnight at 50°C to get a yellow crystalline powder of FITC-labeled ZIF-8 nanoparticles.

2.2. Characterization of the nanoparticles

The crystallinity of the powder was analyzed using an X-ray diffractometer (Bruker AXS D8 Advance, Massachusetts, United States of America [USA]). The Brunauer–Emmett–Teller surface area and pore size distribution were evaluated through gas adsorption studies using a surface area and pore size analyzer (Quantachrome Instruments NOVAtouch®LX2, Anton-Paar, USA). The nanoparticle size and morphology were studied using scanning electron microscopy (SEM; NOVA Nano SEM 450, FEI, USA) and transmission electron microscopy (TEM; JEM-2100F, JEOL USA, Inc., USA). Photoluminescence (PL) emission was investigated using a fluorescence spectrometer (Horiba FluroMax®-4, Horiba Scientific, USA).

2.3. Animal housing and husbandry

The animal model for the *in vivo* study consisted of 48 adult male Swiss albino mice (6–8-week-old, 24–28 g) obtained from the animal house of the Department of Biochemistry, University of Kerala. The animals were housed in separate polypropylene cages with stainless steel grill lids and maintained under standard conditions at an ambient temperature of 22 ± 3°C and relative humidity of 50 ± 10% with a 12:12 h light/dark cycle throughout the experimental period. The animals had access to the commercially available standard pellet diet (Amrut Laboratory Animal Feed, Krishna Valley Agrotech LLP, India) and filtered drinking water *ad libitum*. They were acclimatized for one week before the experiment started. Individual animals were identified using a picric acid mark on the body. Each animal cage was recognized with specifications, including name, experiment number, animal number, commencement date of the experiment, and end of the experimental period. The experimental protocols were reviewed and approved by the Institutional Animal Ethics Committee (IAEC), University of Kerala (Registration Number-218/GO/ReBi/S/2000/Committee for the Purpose of Control and Supervision of Experiments on Animals [CPCSEA]) constituted per the guidelines of the CPCSEA, Department of Animal Husbandry and Dairying, Ministry of Fisheries, Animal Husbandry and Dairying, India. The IAEC sanction order number for the animal study was IAEC-KU-03/2012-13-BC-AA(31).

2.4. Toxicity evaluations

The toxicity of the nanoparticles was evaluated using acute and sub-acute toxicity studies according to the guidelines of the Organization for Economic Co-operation and Development in the animal house, Department of Biochemistry, University of Kerala, following Good Laboratory Practices. Adult male Swiss albino mice (24–28 g) were acclimatized to laboratory conditions for seven days before the beginning of the experiment. Each animal was given a unique identification number and fur marked with picric acid. Before administering nanoparticles, the animals were weighed using a calibrated balance. The weight of the animals, as well as their food and water consumption, was recorded daily throughout the experimental period. The time for providing the feed was fixed, and the animals were observed in their cages daily for mortality and any signs of toxic effects. The effect of treatment on the general health of the animals, body weight, and behavior was also recorded. Mice were deprived of feed for 6 h before and 3 h after the administration of the test compound.

Acute toxicity was measured *in vivo* after the administration of a single high dose. In our study, different groups of mice were administered IP injections of various dosage levels of nanoparticles (25, 50, 100, 500, and 1,000 mg/kg body weight).[10] The observations of behavioral changes were made at 10, 30, 60, and 120 min, as well as at 4, 6, and 24 h. Animals were evaluated for signs of toxicity, lethargy, behavioral modifications, morbidity, body weight changes, and food consumption. The mortality in each group was recorded after seven days. At the dosages of 500 and 1,000 mg/kg body weight, a 100% mortality rate was observed, whereas only 50% mortality was observed at a dose of 100 mg/kg body weight. No mortality was reported at low dosages, such as 25 and 50 mg/kg body weight. Based on the observations, the lethal dose-50 (LD_{50}) value was determined to be 100 mg/kg body weight.

For sub-acute toxicity studies, animals were divided into six groups (a control group, four treated groups, and a positive control group), each containing six mice. Nanoparticles in different fractional doses of the LD_{50} (1/40, 1/20, 1/10, and 1/5) in phosphate-buffered saline (PBS) were administered through IP injection at a prefixed time daily to the different groups of mice (Groups II–V) for 14 consecutive days. In contrast, the control (Group I) was treated with PBS alone.[11] The positive control (Group VI) was administered with a single IP injection of CP (40 mg/kg body weight) 18 h before sacrifice. The animals were sacrificed on the 15th day by cervical dislocation, after which blood, skin, and vital organs were collected. The blood samples were analyzed for biochemical and hematological parameters. Organs such as the liver, kidney, skin, and spleen were examined for macroscopic lesions and were fixed in 10% neutral buffered formalin for histopathological examination using hematoxylin and eosin (H&E) staining.

2.5. Evaluation of the biodistribution of nanoparticles

A total of 12 Swiss albino mice were administered with FITC-labeled ZIF-8 nanoparticles (10 mg/kg body weight) in PBS through IP injection. After the injection, the animals were sacrificed by cervical dislocation at different time intervals (4,

8, 12, and 24 h, $n = 3$ at each time point). Blood and internal organs were collected for further studies. Saline was added to each organ tissue with a threshold volume to its weight and homogenized using a mortar and pestle, followed by centrifugation (Eppendorf 5804 R, Eppendorf AG, Hamburg, Germany) at 12,000 rpm for 10 min to collect the supernatant. The fluorescence intensity of these supernatants was measured using a spectrofluorimeter (Horiba FluroMax®-4, Horiba Scientific, USA) at excitation and emission wavelengths of 485 nm and 528 nm, respectively.[12] For comparison, a standard fluorescence curve of FITC in methanol was prepared. The concentration of the FITC-conjugated nanoparticles in different organs can be quantitatively determined by comparing the obtained fluorescence intensity of supernatants with the standard fluorescence curve of FITC.

2.6. Analyses of enzymes, oxidative stress markers, and protein content

The cyclooxygenase (COX)-2 assay was performed using the thiobarbituric acid (TBA) method.[13] Lipooxygenases (LOX; 5-LOX and 15-LOX) were assayed using the method described by Axelrod *et al.*,[14] and myeloperoxidase (MPO) activity was estimated with the method proposed by Bradley *et al.*[15] Nitric oxide synthase (NOS) was quantified using the method described by Salter *et al.*[16] The level of catalase (CAT) was assayed using the method from Claiborne *et al.*'s[17] study, and superoxide dismutase (SOD) was measured following the method from the study conducted by Kakkar *et al.*[18] The reduced glutathione (GSH) content was determined through the procedure described by Patterson *et al.*,[19] and the level of glutathione-*S*-transferase (GST) was estimated with the method proposed by Habig *et al.*[20] The activity of glutathione peroxidase (GPx) was determined with the method from Mohandas *et al.*'s[21] study, while that of glutathione reductase (GRd) was measured with the procedure of Carlberg *et al.*[22] The levels of lipid peroxidation, indicated by malondialdehyde (MDA) content, in different tissues were measured using the TBA-reactive substances (TBARS) assay as described by Buege and Aust.[23] Protein quantification was performed using the method described by Lowry *et al.*[24]

2.7. Evaluation of the biochemical parameters

Blood samples from mice in each group were collected in polypropylene tubes without anticoagulants. The clotted blood samples were then centrifuged at 3000 rpm for 15 min to separate the serum. Serum glutamic-oxaloacetic transaminase, serum glutamic-pyruvic transaminase, alkaline phosphatase (ALP), acid phosphatase (ACP), N-acetyl-cysteine-activated creatine kinase (CK), and lactate dehydrogenase (LDH) activities were assayed using commercially available kits (Agappe Diagnostics Ltd., Switzerland), per the manufacturer's instructions. The amount of urea, uric acid, creatinine, and bilirubin was determined using a semi-automated clinical chemistry analyzer (Agappe Mispa Viva, Agappe Diagnostics Switzerland GmbH, Switzerland).

2.8. Hematological parameters

Hematology and clinical chemistry studies were performed on mouse blood samples obtained at the time of euthanasia. Blood samples were collected in ethylenediaminetetraacetic acid-coated tubes using cardiac puncture. Different hematological parameters, including white blood cell (WBC) count, red blood cell (RBC) count, hemoglobin (Hb), and platelet (PLT) count, were estimated. The percentage of lymphocytes and neutrophils was also determined. All these parameters were determined using an automated hematological analyzer (ABX Micros 60, HORIBA ABX SAS, France).

2.9. Evaluation of the pro-inflammatory cytokines

Immunotoxicity was evaluated by estimating pro-inflammatory cytokines, such as interleukin-6 (IL-6) and tumor necrosis factor-alpha (TNF-α), in the serum of different groups of mice using enzyme-linked immunosorbent assay kits (Origin Diagnostics and Research, India).

2.10. Histopathological evaluation of the vital organs

The control and treated animals were sacrificed at the end of the study period, and the organs, including liver, kidney, skin, and spleen, were rapidly dissected and washed in sterile PBS. The isolated organs were trimmed into small pieces and preserved in 10% neutral buffered formalin for 24 h. The specimens were successively dehydrated using 70%, 95%, and 100% alcohol for 1, 2, and 3 h, respectively, with alcohol replaced every hour. Tissues were then defatted by treating twice with xylene, each for an hour. Infiltration and impregnation were performed by treating thrice with paraffin wax, each time for an hour. Paraffin L-shaped molds were prepared and the specimens were cut into 5–6 μm thick sections using a rotary microtome (Leica RM 2235, Leica Biosystems Nussloch GmbH, Germany) and stained using H&E. The sections were mounted using dibutylphthalate polystyrene xylene and the histopathological evaluation of organ sections was conducted using a microscope (Olympus CX21i, Olympus Corporation, Japan).

2.11. Statistical analysis

The results were expressed as the mean ± standard deviation of six replicates and analyzed using GraphPad Prism software (version 8.0, GraphPad Software Inc., USA). One-way analysis of variance was used for the repeated measurements, and the differences were considered statistically significant if $p<0.05$.

3. Results

3.1. Characterization studies

Basic characterization studies of the nanoparticles, including X-ray diffraction, SEM, TEM, and PL emission spectrum, are shown in the supplementary file. X-ray diffraction shown in Figure S1A confirms the typical sodalite morphology of the nanoparticles, and SEM shown in Figure S1B confirms the do-decahedral shape of the nanoparticles with an average size of 65–70 nm. The high-resolution TEM image of FITC-labeled ZIF-8 shown in Figure S2A confirms the do-decahedral shape of the nanoparticles with a size of 70 nm. The rings in the selected area electron diffraction pattern (Figure S2B) correspond to the different crystal planes of ZIF-8. The PL emission spectrum of pure ZIF-8 and FITC-labeled ZIF-8 nanoparticles at an excitation wavelength of 340 nm is shown in Figure S3. Pure

ZIF-8 nanoparticles did not produce any emission in the visible region, as indicated by the red line, whereas the FITC-labeled nanoparticles exhibited a strong emission peaked at 528 nm. The green emission by FITC-labeled ZIF-8 nanoparticles corresponds to the typical emission due to the incorporated FITC in the ZIF-8. Hence, the fluorescence emission spectrum confirmed the incorporation of FITC into the ZIF-8, thereby offering fluorescence probing of the nanoparticles.

3.2. *In vivo* toxicity assessment

The *in vivo* toxicity assessment is usually performed in animal models using biodistribution studies, analysis of hematological parameters, estimation of serum enzymes, and histopathological studies.

3.2.1. Biodistribution studies

Biodistribution studies examine the localization of nanoparticles in various organs. The typical green fluorescence of FITC was utilized to estimate the percentage dose of FITC-labeled ZIF-8 nanoparticles in different organs. The standard curve and the linear regression equation for the fluorescence of FITC in methanol are shown in **Figure 1**. Comparison of the fluorescence intensity obtained from blood and tissue supernatants with the standard fluorescence curve yielded the distribution pattern of nanoparticles post IP injection. In addition, the time-dependent (4, 8, 12, and 24 h) distribution pattern of nanoparticles was evaluated.

The percentage dose of nanoparticles in different organs at various time points is depicted in **Figure 2**. A significant proportion of nanoparticles was found in the blood (34.31 ± 1.67%) at an earlier time (4 h). As time elapsed, the concentration was found to decrease gradually to 4.53 ± 1.05% at 24 h. A small accumulation was observed in the liver (3.62 ± 1.08%), followed by the kidney (2.61 ± 0.76%), skin (1.36 ± 0.29%), and spleen (0.86 ± 0.25%). The deposition of the nanoparticles declined to 0.08 ± 0.03% (liver), 0.01 ± 0.009% (kidney), 0.005 ± 0.003% (skin), and 0.006 ± 0.005% (spleen) at 24 h. At all the time points, a maximum distribution of nanoparticles was detected in the blood, indicating systemic blood circulation. The results demonstrated that nanoparticles accumulated in trace amounts in major organs of normal mice and were eliminated systematically. This confirmed the reduced organ toxicity induced by the nanoparticles.

3.2.2. Biochemical parameters

To study the *in vivo* toxicological effects of exposure to nanoparticles, the evaluation of biochemical, hematological, and histopathological responses was conducted in mice at different doses. Initially, various biochemical parameters that contribute directly to detecting, quantifying, and understanding the noteworthy effects of nanoparticle exposure to vital organs were investigated. Hepatic injury can be diagnosed using biochemical markers, such as alanine transaminase (ALT), aspartate aminotransferase (AST), ALP, and bilirubin. Elevation in the serum enzyme level and enhancement in both total and conjugated bilirubin levels are regarded as relevant markers of liver toxicity and gross liver function, respectively. When the liver is damaged, these parameters will be secreted excessively into the bloodstream.[25]

Figure 3 shows AST, ALT, ALP, and ACP levels in different groups of mice. The enzyme ALT is primarily localized to the cytosol of hepatocytes. AST is present in both mitochondria and cytosol of a wide variety of tissues, including the heart, skeletal muscle, kidney, brain, and liver. Therefore, a large amount of mitochondrial AST is present in serum after extensive tissue necrosis, and hence it is preferred over ALT for the diagnosis of liver damage.[26,27] ALP is primarily secreted from the liver and bones; high levels of ALP indicate liver or bone disorders.[28] ACP is a lysosomal marker enzyme produced in the liver, spleen, bone marrow, and prostate gland. An elevated level of ACP can be detected during infection associated with tissue damage.[29] According to the observed results, no significant increase was found in the AST, ALT, ALP, and ACP levels in Groups II and III compared to the control. However, significant increases in ALT and ALP, as well as notable increases in AST and ACP levels, were observed in Groups IV and V. The results showed that the nanoparticles induced little liver toxicity at low doses. Bilirubin also followed a similar pattern as shown in **Figure 4D**, where its level was slightly elevated in Groups IV and V and remained within the normal range in Groups II and III.

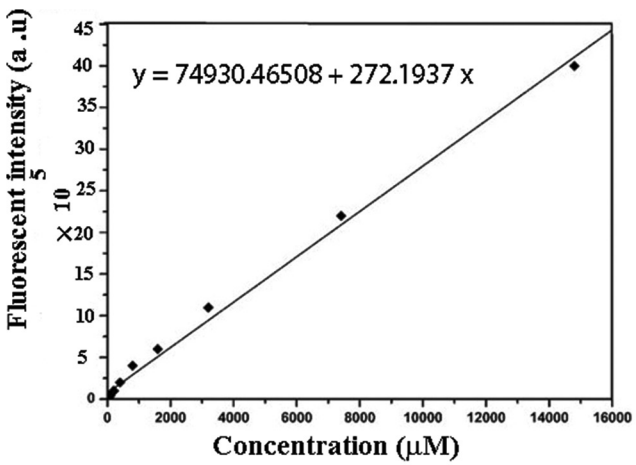

Figure 1. Standard fluorescence curve of fluorescein isothiocyanate

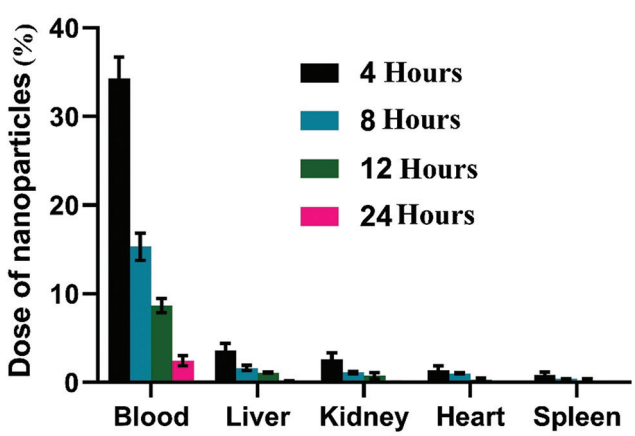

Figure 2. *In vivo* biodistribution of FITC-labeled zeolitic imidazolate framework-8 nanoparticles in Swiss albino mice

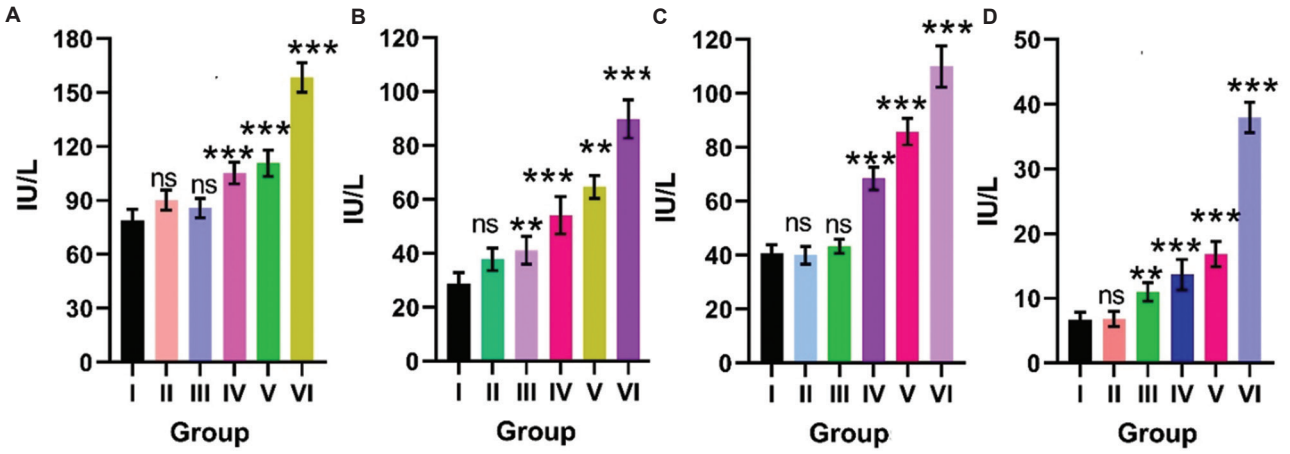

Figure 3. Biochemical marker levels in different groups of mice. (A) Aspartate aminotransferase. (B) Alanine aminotransferase. (C) Alkaline phosphatase. (D) Acid phosphatase. Data are expressed as mean ± standard deviation ($n = 6$).
Notes: $^{**}p<0.01$; $^{***}p<0.001$; ns: non-significant compared to the control group.

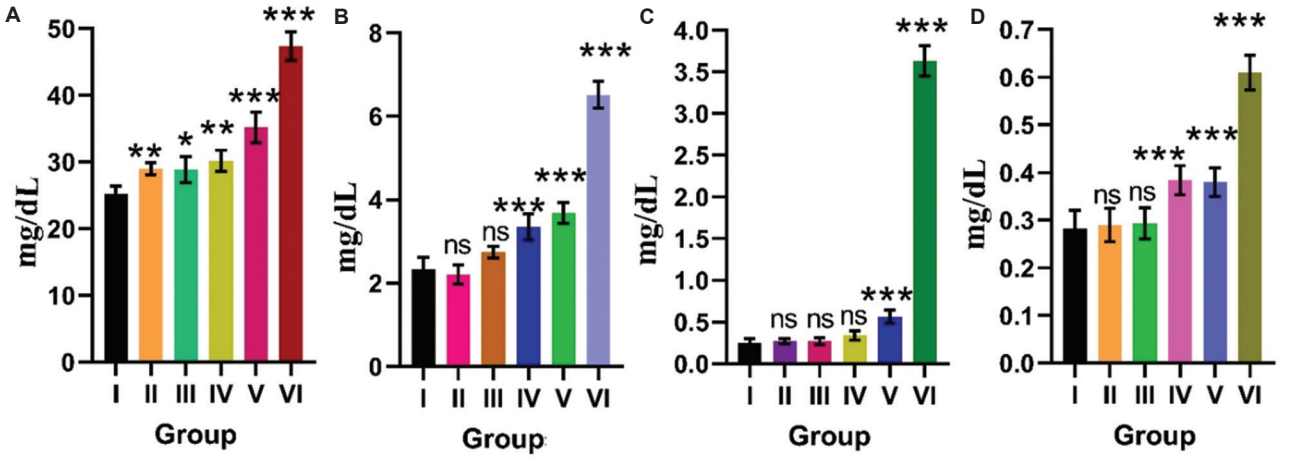

Figure 4. Level of renal parameters in different groups of mice. (A) Urea. (B) Uric acid. (C) Creatinine. (D) Bilirubin. Data are expressed as mean ± standard deviation ($n = 6$).
Notes: $^{*}p<0.05$; $^{**}p<0.01$; $^{***}p<0.001$; ns: non-significant compared to the control group.

3.2.3. Renal parameters

The levels of renal parameters, such as urea, uric acid, and creatinine, increase substantially in renal toxicity.[30-32] The levels of urea, uric acid, creatinine and bilirubin in blood are respectively shown in **Figures 4a-d.** The above parameters exhibited small elevations in Groups IV and V, indicating that the nanoparticles induced negligible nephrotoxicity even at high doses. Uric acid was found to be elevated in Groups IV and V compared to the control, whereas there were no significant elevations in urea and creatinine up to Group IV. However, a slight increase in urea and creatinine was observed in Group V compared to the control. The results demonstrated that administration of low doses of nanoparticles results in negligible renal toxicity.

CK plays a central role in maintaining adenosine triphosphate (ATP) homeostasis. It catalyzes the reversible transfer of the phosphate group from ATP to creatine, forming phosphocreatine. It is primarily found in muscle and brain tissues, where its physiological role is ATP generation for contractile or transport systems. Elevated CK values are observed in cerebrovascular diseases, muscular dystrophy, strenuous exercise, and surgery. LDH is a cytosolic enzyme present in different tissues, and when a disease or a toxin damages tissues, LDH is released into the bloodstream. The levels of CK and LDH (**Figure 5**) in Groups II and III treated with lower doses were observed to be close to those in the control. Both factors were found to be elevated slightly in Groups IV and V treated with higher doses. Generally, the elevated serum CK and LDH levels indicate tissue damage during pathological conditions. The levels of biochemical parameters in the CP-treated positive control (Group VI) indicate severe hepatotoxicity, renal toxicity, and inflammation.

3.2.4. Hematological parameters

Blood, composed of proteins and cells, is the first medium of contact for intravenously injected nanoparticles, and blood cells make up 45% of blood volume. Nanomaterial interactions with blood cells have different effects depending on their intrinsic characteristics, such as surface chemistry and charge. Mature blood cells are produced continuously in the body and

maintained at equilibrium by the hematopoietic system. This system can be easily disturbed by direct and indirect xenobiotic-induced damage. Toxic effects on the hematopoietic system result in alterations of blood and blood-forming tissues. Nanoparticles may induce inflammatory responses and affect the immune system activity, leading to variations in blood cell counts.[33]

Figure 6 shows the blood cell counts in different groups of mice. There were no significant changes in Hb and RBC counts in animals treated with lower doses of nanoparticles. Dose-dependent reduction in Hb count was observed in groups treated with elevated doses. The observed decrease may be due to nanoparticle-induced oxidative stress and concomitant destruction of RBCs. The WBC content was significantly increased in Groups IV and V, which were treated with higher doses. This was due to the modulation of the immune system in response to invading foreign bodies, resulting in phagocytosis.[34] A remarkable reduction in the number of PLTs was observed for Groups IV and V, which is common during inflammation.

Lymphocytes are the primary cells involved in adaptive immunity; they produce antibodies in response to foreign invaders. They are made in the bone marrow, circulate in the blood and lymphatic systems, and reside in various lymphoid organs. Lymphocytes also mediate the four major adaptive immunologic attributes, including specificity, diversity, memory, and self/non-self-recognition. The two major types of lymphocytes are B lymphocytes (B cells) and T lymphocytes (T cells). The B cells are responsible for humoral immunity against extracellular pathogens, whereas T cells are responsible for cellular immunity, which deals with intracellular pathogens. Neutrophils play a central and essential role in inflammation,[35] as neutrophil apoptosis is a crucial step in the resolution of inflammation. During inflammation, activated neutrophils adhere to the vascular endothelium and transmigrate to the extravascular space, releasing reactive oxygen species (ROS), protease enzymes, and large amounts of chemokines.[36] ROS and proteases damage normal tissue and extracellular matrix proteins.[37] **Figure** 7 shows the percentage of lymphocytes and neutrophils. The percentage of lymphocytes exhibited an insignificant elevation in Group IV, whereas Group V showed a significant increase compared to the control group. Regarding the percentage of neutrophils, a remarkable decrease was observed in Groups IV and V compared to the control group. The variations in hematological parameters observed in higher-dose treated groups may be attributed to the inflammatory process. Significant variations in the hematological parameters in Group VI compared to the control group indicated potential hemotoxicity of CP.

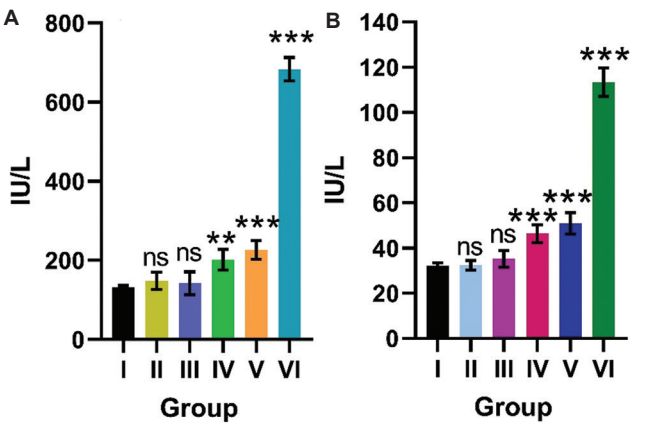

Figure 5. Biochemical marker levels in different groups of mice. (A) Lactate dehydrogenase. (B) Creatine kinase. Data are expressed as mean ± standard deviation ($n = 6$).
Notes: $^{**}p<0.01$; $^{***}p<0.001$; ns: non-significant compared to the control group.

3.2.5. Inflammatory markers

Eicosanoids, derived from polyunsaturated fatty acids (PUFAs), are produced through pathways regulated by various enzymes, including COX-1, COX-2, LOXs (5-LOX, 12-LOX, and 15-LOX), and cytochrome P450. COX or prostaglandin-endoperoxide synthase is the enzyme involved in the formation of prostanoids from arachidonic acid. COX exists in two isoforms, namely COX-1 and COX-2. In many instances, the COX-1 enzyme is produced constitutively (e.g., in gastric mucosa), whereas COX-2 is highly inducible (e.g., at sites

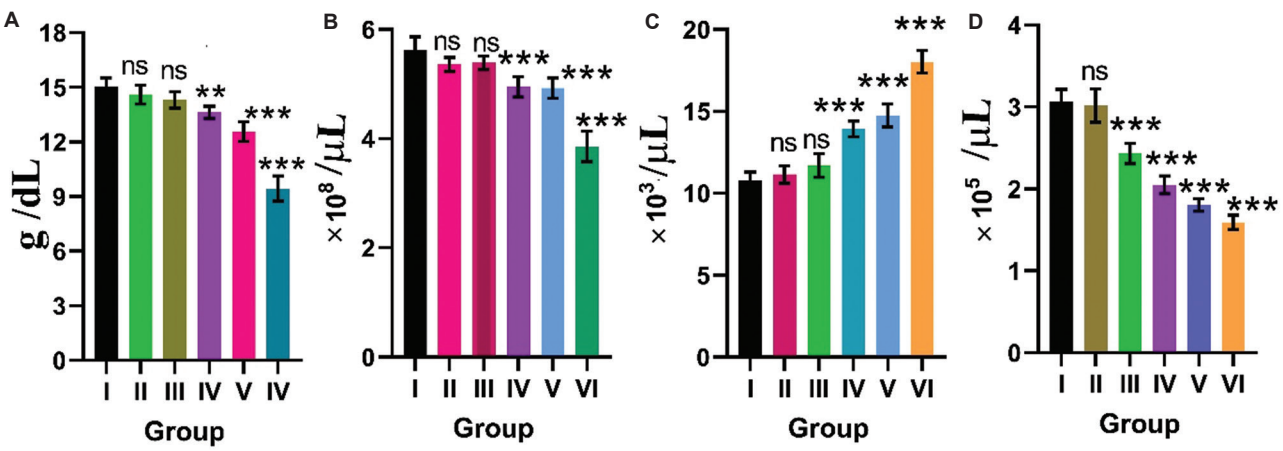

Figure 6. Blood cell counts in different groups of mice. (A) Hemoglobin. (B) Red blood cells. (C) White blood cells. (D) Platelet. Data are expressed as mean ± standard deviation ($n = 6$).
Notes: $^{**}p<0.01$; $^{***}p<0.001$; ns: non-significant compared to the control group.

of inflammation and cancer).[38] The fundamental role of these enzymes is to produce prostaglandins, which serve as local hormones for inducing inflammation, pain, and fever. However, COX-2 is primarily responsible for the formation of prostanoids during inflammation and cancer.[39,40] LOXs are non-heme iron-containing dioxygenases that catalyze the addition of molecular oxygen to unsaturated fatty acids containing a cis, cis-1,4-pentadiene system, converting them to epoxides. 4-hydroperoxy cis-trans-1,3-conjugated pentadienyl moiety is the initial product of this reaction. Based on the position of the introduced hydroperoxide, the three main LOX enzymes are designated as 5-, 12-, and 15-LOX. These enzymes play a key role in cell proliferation, differentiation, and inflammation. During inflammation, 5-LOX initiates the biosynthesis of pro-inflammatory leukotriene lipid mediators. 5-LOX also produces anti-inflammatory lipoxins with the help of 15-LOX.[41] Leukotrienes are produced in leukocytes by the 5-LOX through the oxidation of arachidonic acid and the essential fatty acid, eicosapentaenoic acid. Lipoxins are LOX-derived interaction products of arachidonic acid that play anti-inflammatory roles. They are generated through the action of 5- and 15-LOXs during cell-cell interactions in inflammation via transcellular biosynthesis. Lipoxins are endogenous anti-inflammatory, pro-resolving molecules that play a vital role in reducing excessive tissue injury and chronic inflammation.[42] In short, the activities of all the enzymes above are enhanced during inflammation. **Figure 8** shows the enzyme levels in different groups of mice. The activity of these enzymes in Group II was found to be similar to that of the control group, while only a slight increase was observed in Groups III and IV. A sharp rise in the enzyme activities was observed only in Group V. The inflammatory marker enzymes were found to be markedly elevated in the positive control group. The obtained results showed that the administered nanoparticles induced a negligible inflammatory response at lower doses.

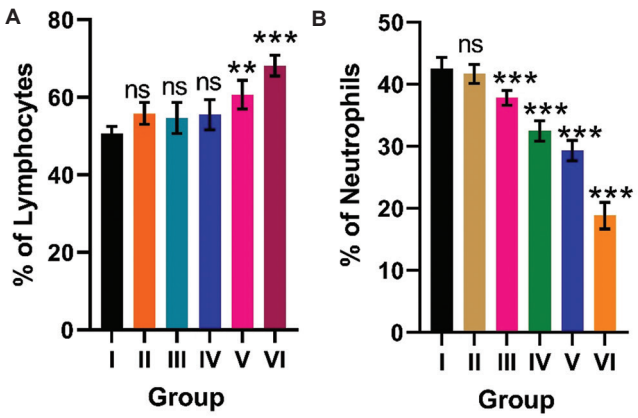

Figure 7. Percentage of leukocytes in different groups of mice. (A) Lymphocytes. (B) Neutrophils. Data are expressed as mean ± standard deviation ($n = 6$).
Notes: **p<0.01; ***p<0.001; ns: non-significant compared to the control group.

3.2.6. Oxidative and nitrosative stress enzymes

MPO is a heme-containing peroxidase enzyme found in the azurophilic granules of the lysosomes of leukocytes, such as neutrophils, monocytes, and tissue macrophages. It catalyzes the production of hypochlorous acid from hydrogen peroxide and a chloride anion. MPO oxidizes tyrosine to a tyrosyl radical, where hydrogen peroxide functions as an oxidizing agent. It can also be regarded as a marker and mediator of inflammation and oxidative stress, as it catalyzes the formation of several ROS.[43] Upon neutrophil activation, primary granules containing MPO will fuse with the plasma membrane to secrete contents into the extracellular medium. Enhanced MPO activity indicates increased neutrophil infiltration and inflammation. Nitric oxide (NO) is another mediator of inflammatory response due to its ability to influence the phenotype of inflammatory cells and its contribution to the formation of reactive nitrogen products.[44] NO is produced in a reaction catalyzed by NOS, in which oxygen and L-arginine are converted into L-citrulline and NO. It is involved in host defense, activation of regulatory proteins, and direct covalent interaction with functional biomolecules. It regulates the functional activity, growth, and death of many immune and inflammatory cell types, including

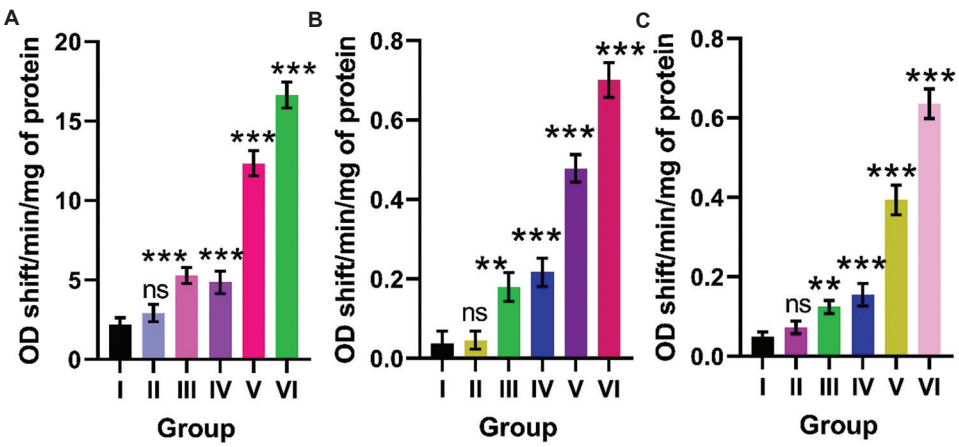

Figure 8. Activity of enzyme levels in different groups of mice. (A) COX-2. (B) 5-LOX. (C) 15-LOX. Data are expressed as mean ± standard deviation ($n = 6$).
Notes: **p<0.01; ***p<0.001; ns: non-significant compared to the control group.
Abbreviations: COX: Cyclooxygenase; LOX: Lipoxygenase; OD: Optical density.

macrophages, T-lymphocytes, antigen-presenting cells, mast cells, neutrophils, and natural killer cells. NOs are oxidized to reactive nitrogen species at elevated concentrations, which in turn mediate the majority of the immunological phenomena.[45] **Figure 9** shows the activities of MPO and NOS. It was observed that both parameters were significantly elevated in Groups IV and V, indicating the inflammation and oxidative stress induced by the nanoparticles at higher concentrations.

3.2.7. Antioxidant enzymes

Antioxidant systems are effective in stabilizing or inactivating ROS, as well as the oxidation products of phospholipids and PUFAs, such as lipid peroxides. These mediate the catalytic transformation of ROS, such as hydroxyl radical, superoxide anion radical, hydrogen peroxide, singlet oxygen, NO radical, and hypochlorite radical, into stable non-toxic molecules. These systems are critical in preventing oxidative stress and maintaining optimal cellular health. Various enzymatic and non-enzymatic antioxidants are involved in the oxidative defense mechanism to equilibrate the redox potential of living cells. Major antioxidant enzymes responsible for eliminating free radicals from the body include SOD, CAT, GPx, GST, and GRd. For non-enzymatic antioxidants, reduced GSH occupies a significant position in neutralizing oxidative species in the intracellular compartments. SOD and CAT are remarkably efficient in eliciting defense against ROS-mediated damage.[46] SOD scavenges superoxide radicals ($O_2 \bullet^-$) by catalyzing the conversion of two of these radicals into hydrogen peroxide and molecular oxygen. This decreases the $O_2 \bullet^-$ level to prevent cell damage resulting from its excessive concentration. The oxidized form of SOD is reduced by superoxide to form oxygen. The reduced form of this enzyme subsequently reacts with a second superoxide ion to form peroxide, which takes up two protons along the reaction pathway to produce hydrogen peroxide.[47] CAT scavenges the hydrogen peroxide generated by SOD and other processes. It is a heme prosthetic group-containing enzyme that catalyzes the dismutation reaction of H_2O_2 into water and molecular oxygen. Abnormalities in CAT activity result in pathogenesis and inflammation, which in turn lead to oxidative stress.[48] **Figure 10** shows the CAT activity in the liver tissue of different groups of mice. A small decrease in CAT activity was observed in all groups compared to the control group, but the dose-dependent reduction was insignificant in Groups II to V. The SOD activity of the liver and kidney is shown in **Figure 11**. Liver tissue of Groups II and III exhibited only mild changes in the SOD levels. In contrast, those of Groups IV and V showed a significant decrease compared to those of the control group. Regarding the SOD levels in kidney tissue, significant changes were observed in all treated groups (Groups II to V).

GSH is a tripeptide with a free sulfhydryl group responsible for the detoxification of peroxides, such as hydrogen peroxide or lipid peroxides. It, thus, combats oxidative stress by reducing ROS to harmless forms. During detoxification, GPx activates the oxidation of GSH into oxidized GSH (GSSG). GSSG will be recycled into reduced GSH by the enzyme GRd present in cells.[49] The reducing power is provided by nicotinamide adenine dinucleotide phosphate (NADPH), which in turn was produced by the enzyme glucose-6-phosphate dehydrogenase

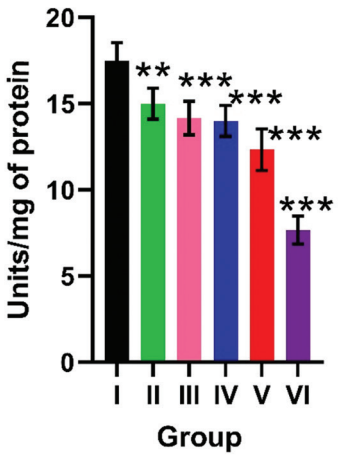

Figure 10. Catalase activity in the liver tissue of different groups of mice. Data are expressed as mean ± standard deviation ($n = 6$)
Note: $^{**}p<0.01$; $^{***}p<0.001$; ns: non-significant compared to the control group

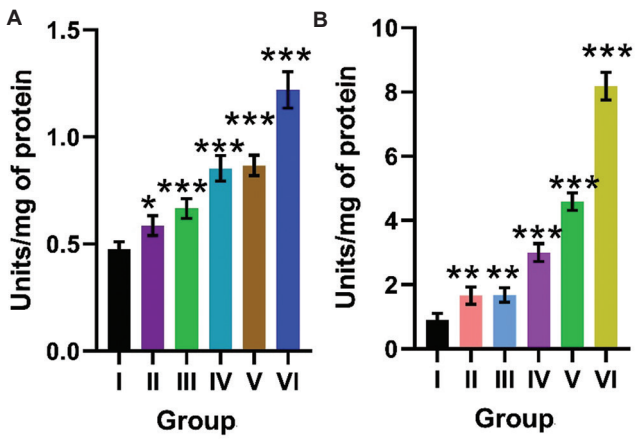

Figure 9. Activity of oxidative and nitrosative stress enzymes in different groups of mice. (A) Myeloperoxidase. (B) Nitric oxide synthase. Data are expressed as mean ± standard deviation ($n = 6$).
Notes: $^{*}p<0.05$; $^{**}p<0.01$; $^{***}p<0.001$.

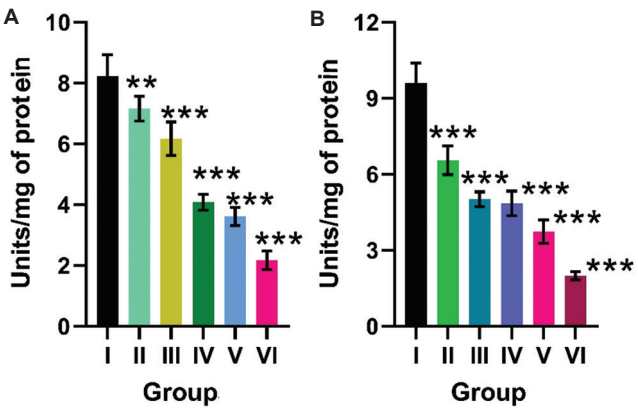

Figure 11. Superoxide dismutase activity in the tissues of different groups of mice. (A) Liver. (B) Kidney. Data are expressed as mean ± standard deviation ($n = 6$)
Note: $^{**}p<0.01$; $^{***}p<0.001$; ns: non-significant compared to the control group

in the hexose monophosphate shunt pathway. It has been reported that cells with low levels of glucose-6-phosphate dehydrogenase are susceptible to oxidative damage. Oxidative stress is more severe in RBCs as they lack mitochondria and are devoid of an alternative supply of NADPH. GSH is vital for maintaining the structure of Hb in RBCs. GSH serves as a sulfhydryl buffer that keeps the Hb residues in reduced sulfhydryl form. Without adequate levels of GSH, the Hb sulfhydryl groups cannot be maintained in the reduced form, leading to the formation of aggregates known as "Heinz bodies" on membranes as a result of the cross-linking of Hb molecules. **Figure 12** shows the GSH level in the liver and kidneys. Large variations in the GSH levels were observed in the kidney tissues in Groups IV and V, whereas in Groups II and III, the GSH levels remained within the normal range. For liver tissues, a remarkable decrease was observed in Group V only. The observed depletion of GSH after treatment with higher doses was probably due to an increased utilization of GSH in both enzymatic and non-enzymatic reactions.[50,51]

GPx, a selenoenzyme, catalyzes the reduction of hydrogen peroxide and organic peroxides by GSH. The activity of GPx in the liver and kidney tissues is shown in **Figure 13**. Significant changes in GPx level were observed in the kidney for Groups IV and V, whereas Groups II and III exhibited insignificant variation from the control value. For the liver, Group V exhibited a sharp decline in GPx level compared to the control group. GRd, which uses NADPH as the electron source, reduces GSSG to GSH.

The activity of GRd is shown in **Figure 14**, where the levels in the kidney tissue of Groups II, III, and IV were found to be appreciably close to those in the control group. A notable decrease in GRd activity was observed in the liver tissue for Groups III, IV, and V.

GSH S-transferases are an abundant family of enzymes that catalyze the conjugation of GSH to foreign materials, usually resulting in detoxification. They catalyze the conjugation of GSH to electrophilic centers on a wide variety of compounds via the sulfhydryl group, thereby making the compounds more water-soluble. This process detoxifies endogenous compounds and enables the breakdown of xenobiotics. The conjugate will then be considerably less toxic than the unconjugated precursor compound.[52] The variation in the level of GST in the liver and kidney of different groups of mice is shown in **Figure 15**. Based on the figure, there was no considerable reduction in GST activity in the kidney tissue of Groups II and III, whereas in Groups IV and V, the activity was decreased remarkably. Regarding the GST expression in the liver, Group II showed activity similar to the control group. A modest decline in Group III and sharp decreases in Groups IV and V were observed. Depleted GSH, GPx, GRd, and GST activities at higher doses suggest increased utilization of GSH in the cytochrome P450-mediated detoxification mechanism. The CP-treated group exhibited a depleted level of all the antioxidant enzymes, indicating potential toxicity.

Functional damage to cells under oxidative stress is not only caused by oxygen free radicals or unbalanced redox potential, but also by the enhanced lipid peroxidation. The oxidation

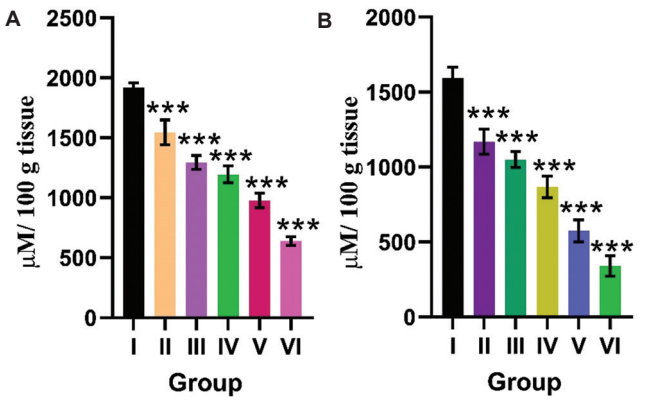

Figure 12. Reduced glutathione level in tissues of different groups of mice. (A) Liver. (B) Kidney. Data are expressed as mean ± standard deviation ($n = 6$).
Note: *** $p<0.001$.

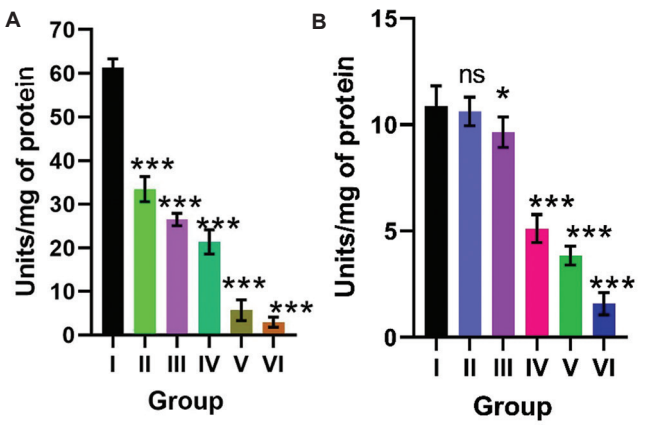

Figure 13. Glutathione peroxidase activity in tissues of different groups of mice. (A) Liver. (B) Kidney. Data are expressed as mean ± standard deviation ($n = 6$).
Notes: *$p<0.05$; *** $p<0.001$; ns: non-significant compared to the control group.

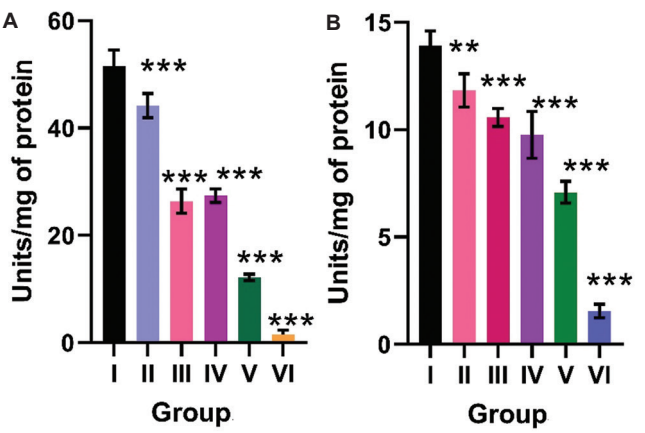

Figure 14. Glutathione reductase activity in tissues of different groups of mice. (A) Liver. (B) Kidney. Data are expressed as mean ± standard deviation ($n = 6$).
Notes: **$p<0.01$; ***$p<0.001$.

of phospholipids and PUFAs results in the formation of lipid peroxides. Lipid peroxidation is an important index of oxidative stress, and MDA is one of its degradative products.[53,54] The other product is 4-hydroxy-2-nonenal. The MDA present in different tissues was measured using the TBARS assay. **Figure 16** shows the MDA levels in the liver and kidneys of the control and treated groups. Only small variations in MDA levels in the liver tissue were observed across all groups. In contrast, a remarkable rise in MDA levels was observed in the kidney tissue of Group V. The increase in MDA levels in liver and kidney tissues indicates the formation of hydroxyl radicals, which are associated with lipid peroxidation in tissues. A sharp elevation in lipid peroxidation level in the CP-treated group was observed compared to the control group.

Here, we could observe that at higher doses, there was a reduction in the activity of potential antioxidant enzymes, such as GSH and MDA. The metallic nature of nanoparticles, as well as the presence of transition metals, might have enhanced the generation of ROS, which led to oxidative stress. This created an imbalance between the antioxidants and the free radicals, where ROS production overwhelmed the cell's natural defense mechanisms, leading to a depletion of the activity of major enzymes.[55,56] In a state of normal equilibrium, there is a balance between free radicals that are generated and used. The uncontrolled production of hydrogen peroxide and oxide-free radicals results in severe oxidative stress and disrupts the natural antioxidant systems, thereby reducing the activity of potential enzymes. A similar study that administered silver nanoparticles resulted in a significant reduction in the activities of GST, CAT, and SOD in animal models.[57] The report related to CP-induced toxicity showed that CP treatment caused lipid peroxidation and suppressed tissue and serum levels of GSH, GPx, GRd, SOD, and CAT.[58] In that study, the biochemical, hematological, and enzymatic parameters in the CP-treated group indicated severe toxicity and inflammation. Our investigation proved that, at a lower dose, the nanoparticles were not associated with any serious adverse effects.

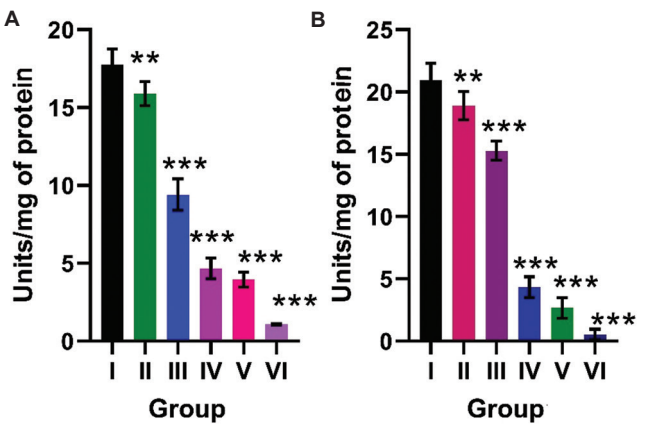

Figure 15. Glutathione-S-transferase activity in tissues of different groups of mice. (A) Liver. (B) Kidney. Data are expressed as mean ± standard deviation ($n = 6$).
Note: $^{**}p<0.01$; $^{***}p<0.001$.

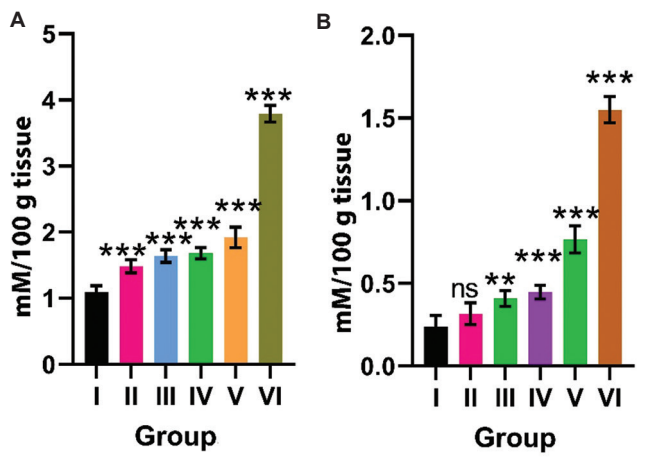

Figure 16. Malondialdehyde level in (A) liver and (B) kidney tissues of different groups of mice. Data are expressed as mean ± standard deviation ($n = 6$).
Notes: $^{**}p<0.01$; $^{***}p<0.001$; ns: non-significant compared to the control group.

3.2.8. Immunotoxicity markers

Cytokines are proteins synthesized by different types of cells, including immune cells. They play a major role in the modulation and regulation of the immune system. They also perform pleiotropic functions and are generally recognized as biomarkers of immunotoxicity.[59] Therefore, measuring the expressions of cytokines, especially the pro-inflammatory cytokines, helps in evaluating the nanoparticle-induced immunotoxicity, where high levels of cytokines are usually reported. **Figure 17** illustrates the expression levels of two prominent pro-inflammatory cytokines, namely IL-6 and TNF-α, which promote innate immunity and eliminate pathogens. They activate functions of inflammatory cells during acute inflammatory responses and increase the vascular permeability, which causes swelling and redness. IL-6 is responsible for fever reactions, whereas the vasodilator effects of TNF-α are attributed to the marked hypotension seen in septic shock. The expression of TNF-α was comparable in

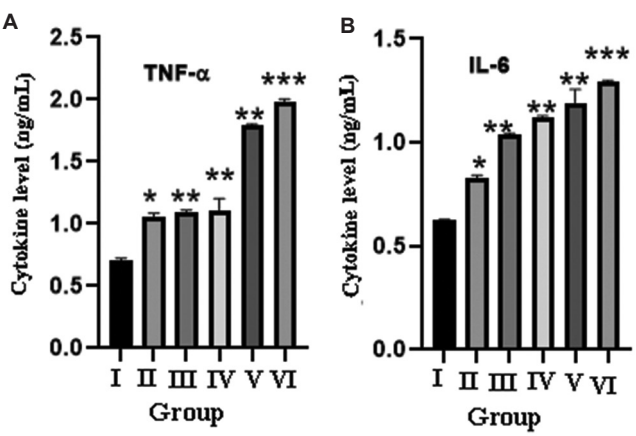

Figure 17. Expression of TNF-α and IL-6 in different groups of mice. Data were expressed as mean ± standard deviation ($n = 6$).
Note: $^{*}p<0.05$; $^{**}p<0.01$; $^{***}p<0.001$.
Abbreviations: PC: Positive control, IL-6: Interleukin-6; TNF- α: Tumor necrosis factor-alpha.

Groups II, III, and IV compared to the control group, whereas a notable increase was observed in Group V. In the case of IL-6, a dose-dependent increment of IL-6 was observed from Groups II to V. The results indicated that low doses of nanoparticles do not induce immunotoxicity.

3.3. Histopathological analysis

Histopathological analysis allows for the detailed microscopic evaluation and histological assessment of tissue interactions with the nanoparticles.[60] The histopathology of the liver, kidney, skin, and spleen of the control and nanoparticle-treated groups is shown in **Figure 18**.

Histopathological analyses of different organs did not suggest any acute toxicity in the treatment groups compared to the control. No apparent histopathological abnormalities or lesions were observed in the liver, kidney, skin, and spleen sections of Groups II and III. Groups II and III exhibited normal organ texture as in the control group. The liver section showed hepatic lobules composed of cords of liver cells separated by sinusoids, and the portal triads were well seen. Phagocytic Kupffer cells were seen scattered along the walls of sinusoids. Each hepatocyte had a centrally located nucleus and a glycogen-rich pink cytoplasm. Hepatocytes were normal, with no serious signs of inflammatory response. No evidence of inflammation, necrosis, hemorrhage, or cholestasis in liver tissue was noted. The kidney sections showed healthy renal cortex and renal corpuscles, which consisted of Bowman's capsules with glomeruli, and the convoluted tubules were lined by renal epithelium. The renal interstitium was found to be free from edema or inflammation. The spleen sections exhibited normal splenic structure with healthy lymphoid follicles and sinuses, and the white pulp was found to be more

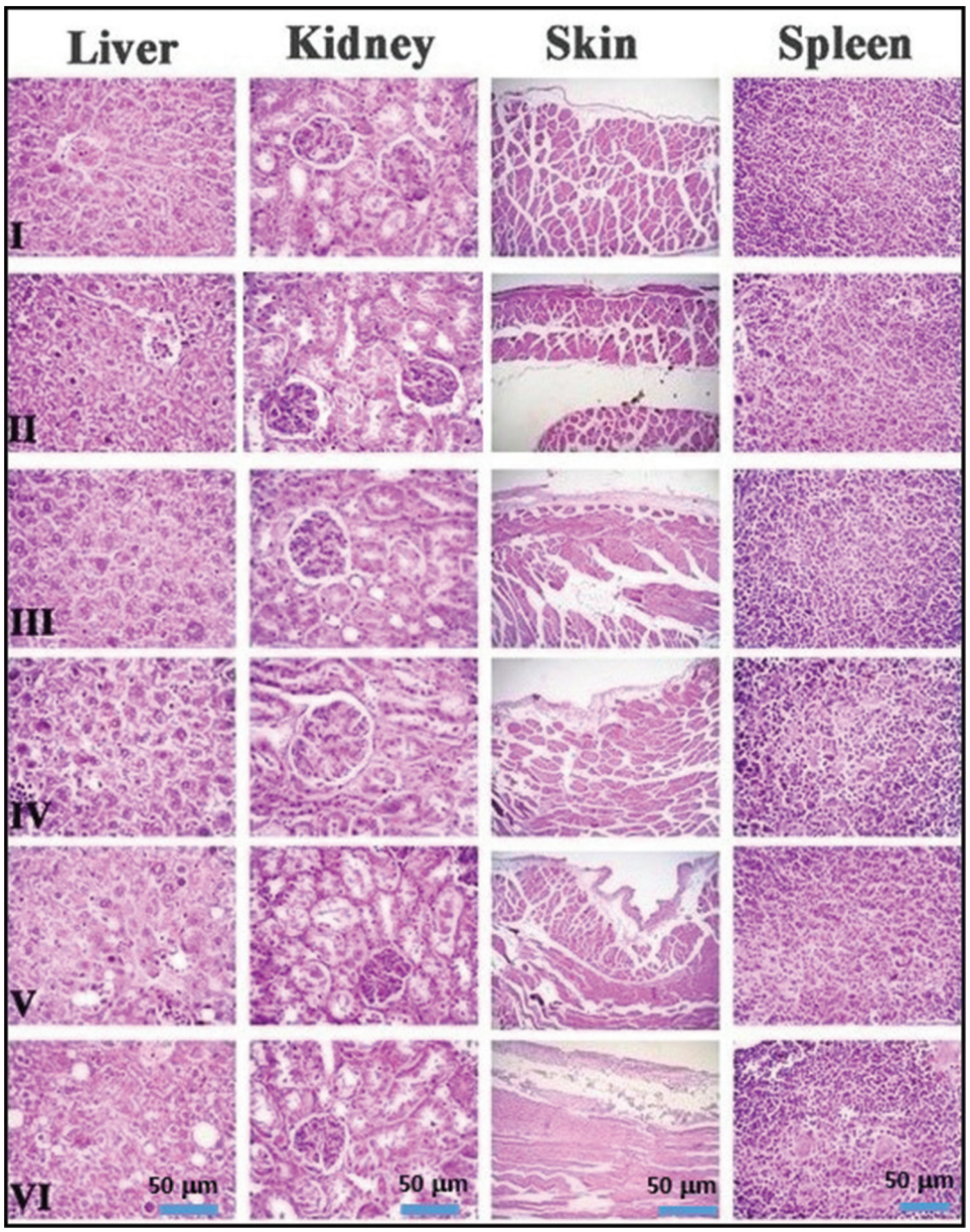

Figure 18. Hematoxylin- and eosin-stained images of liver, kidney, skin, and spleen sections of different groups of mice. Scale bar: 5 µm; magnification: 40×. I–VI indicate group numbers.

well-defined than the red pulp. In addition, lymphatic nodules with germinal centers surrounded by rings of densely packed lymphocytes were observed. Skin sections exhibited normal skin histology, with dermis showing hair follicles, sebaceous glands, and sweat glands. Thus, the histological examination did not show any adverse symptoms of toxicity in the kidney, liver, spleen, and skin of Groups II and III. Necrosis was absent in all the histological samples analyzed.

The liver section of Group IV mice consisted of hepatic parenchymal lobules and portal triads, but showed mild anisokaryosis and hyperchromatosis. Similarly, no signs of inflammation, necrosis, hemorrhage, or cholestasis were observed. The kidney and spleen sections have normal histology similar to that of the control. The kidney section showed healthy glomeruli and tubules with abundant corpuscular space. Furthermore, mild hyperplasia in the dermis and moderate inflammatory cell infiltration in the hypodermis were observed. Vascular dilation and edema were detected in deeper tissue.

The liver cells of Group V exhibited moderate anisokaryosis, hyperchromatosis, mild inflammatory cell infiltration, and fatty changes. Kupffer cells were found to be swollen, and dispersed apoptosis was observed. The spleen section had normal histology but with slight congestion of the red pulp. The skin epithelium displayed moderate hyperplasia; dermis and hypodermis became edematous and showed moderate inflammatory cell infiltration. In Group V, a moderate level of inflammation was observed in the kidney, liver, and skin, while no remarkable changes were observed in the spleen histology. The observed results matched well with previous reports where nanoparticle treatment induced severe changes in the histology of the mice's organs.[61,62] The parenchymal cells of the liver in the positive control group showed mild to moderate nuclear anisokaryosis. Hepatocytes exhibited cellular dysplasia and focal infiltration of inflammatory cells. The kidney section showed loss of normal renal architecture, infiltration of inflammatory cells, and fatty changes with cell swelling. The interstitial tissues were edematous, indicating mild glomerulonephritis. The infiltration of inflammatory cells was visible around the distorted glomeruli and dilated tubules. Skin epithelium showed moderate hyperplasia. The dermis and hypodermis became edematous, showing moderate inflammatory cell infiltration. The deeper tissue exhibited vascular dilation, while the spleen section showed diffuse white pulp and distorted lymphatic architecture, with the lymphoid follicles surrounded by giant macrophages. The histology of the positive control depicts typical indications of organ toxicity and inflammation.

4. Discussion

The study revealed that the hematological, biochemical, inflammatory, antioxidant, and immunotoxicity parameters of mice injected with lower doses of nanoparticles are comparable to those of the positive control mice. The histopathological evaluation of major organs also assured that the FITC-labeled ZIF-8 nanoparticles did not show any marked toxicity at lower doses. The results showed a rise in the induced toxicity parameters when the dosage of nanoparticles increased. This may be due to the increased nanoparticles that overwhelm the body's natural defense and clearance mechanisms, leading to cellular stress or death. Higher doses may lead to high oxidative stress caused by the increased ROS production, damaging DNA, proteins, and membranes. At lower doses, cells neutralize ROS using antioxidants, while at higher doses, ROS levels exceed the cell's capacity, leading to lipid peroxidation, DNA damage, and protein denaturation. The nanoparticles can also physically interact with and damage cellular membranes at higher concentrations. Excess nanoparticles in phagocytic cells (e.g., macrophages) can cause lysosomal rupture, releasing inflammatory mediators. Higher nanoparticle doses provide an increased surface area for interaction, which enhances interactions with biological molecules, offering more binding to proteins (formation of protein corona) and higher potential to adsorb or catalyze harmful reactions. In addition, higher doses can also compromise cell membranes and tight junctions in epithelial/endothelial layers, leading to increased permeability and uncontrolled immune cell infiltration, worsening inflammation. Overall parameters in our study confirm that the safe dosage limit of the FITC-labeled ZIF-8 nanoparticles is 10 mg/kg for future drug delivery in tumor-bearing mice.

Several studies have demonstrated that ZIF-8 nanoparticles exhibit minimal toxicity at lower concentrations when administered via intravenous or IP injections.[63,64] Mao *et al.*[65] reported that nano-ZIF-8 exhibited lower toxicity both *in vitro* and *in vivo*. Kumari *et al.*[66] explored the *in vivo* biosafety of ZIF-8 for intranasal vaccine delivery. The findings of this study are consistent with previous reports on the biocompatibility of ZIF-8 nanoparticles. The current study further supports these conclusions by showing that FITC-labeled ZIF-8 nanoparticles, when administered to Swiss albino mice, did not induce marked changes in hematological, biochemical, oxidative stress, or immunological markers at lower doses. Additionally, when compared to CP, a known chemotherapeutic with established systemic toxicity, the FITC-ZIF-8 nanoparticles exhibited a safer profile. These findings underscore the potential of ZIF-8-based platforms as safe and effective vehicles for targeted drug delivery in cancer therapy.

As a limiting case in our study, we faced difficulty in analyzing the behavioral changes and adaptive immune responses in the mouse. The qualitative estimation of lipid peroxidation, which is to be conducted in future studies, could not be performed using the TBARS assay. *In vivo* toxicity studies should be conducted in tumor mice using the carrier and drug-loaded nanoparticles. This study used only male mice, which may not have accounted for the sex-specific toxic effects in female mice. There are certain general limitations in *in vivo* toxicity testing in mouse models. The limited genetic diversity of laboratory mice may not represent the range of responses observed in a diverse human population from a clinical perspective. Despite genetic similarities, differences in metabolism, physiology, and immune response can also result in inaccurate extrapolation of the results to humans.

5. Conclusions

Fluorescein isothiocyanate-labeled ZIF-8 nanoparticles were synthesized, and their *in vivo* toxicity profile was investigated

in 6–8-week-old Swiss albino mice. *In vivo* toxic effects were evaluated for different doses of the nanoparticles, and the toxicity profile of the nanoparticles was compared with the toxicity level generated by CP. The results of hematological, biochemical, inflammatory, antioxidant, and immunotoxicity markers, and histopathological evaluation showed that the FITC-labeled ZIF-8 nanoparticles did not result in any marked toxicity at lower doses. Therefore, ZIF-8 nanoparticles can be safely employed as a suitable platform for drug delivery in *in vivo* cancer therapy.

Acknowledgement

The authors acknowledge the University Grants Commission, Government of India, for approving the Faculty Development Programme to support the research activities.

Financial support

None.

Conflicts of interest statement

The authors declare they have no competing interests.

Author contributions

Conceptualization: RS; *Data curation*: UA; *Formal analysis:* UA; *Methodology:* RS; *Supervision*: AA; *Writing – original draft:* UA; *Writing – review & editing:* RS. All authors read and approved the final manuscript.

Ethics approval and consent to participate

The experimental protocols were reviewed and approved by the Institutional Animal Ethics Committee (IAEC), University of Kerala (Registration Number-218/GO/ReBi/S/2000/CPCSEA) constituted per the guidelines of the Committee for the Purpose of Control and Supervision of Experiments on Animals (CPCSEA), Department of Animal Husbandry and Dairying, Ministry of Fisheries, Animal Husbandry and Dairying, India. The IAEC sanction order number for the animal study was IAEC-KU-03/2012-13-BC-AA (31).

Consent for publication

Not applicable.

Availability of data

Data are available from the corresponding authors upon reasonable request.

References

1. Parasuraman S. Toxicological screening. *J Pharmacol Pharmacother.* 2011;2(2):74-79. doi: 10.4103/0976-500X.81895
2. Goud NS. Biocompatibility evaluation of medical devices. In: Faqi AS, editor. *A Comprehensive Guide to Toxicology in Nonclinical Drug Development.* Cambridge, MA: Academic Press; 2016. p. 957-973. doi: 10.1016/b978-0-323-85704-8.00030-x
3. Zhao H, Gong L, Wu H, *et al.* Development of novel paclitaxel-loaded ZIF-8 metal-organic framework nanoparticles modified with peptide dimers and an evaluation of its inhibitory effect against prostate cancer cells. *Pharmaceutics.* 2023;15(7):1874. doi: 10.3390/pharmaceutics15071874
4. Tran VA, Lee SW. pH-triggered degradation and release of doxorubicin from zeolitic imidazolate framework-8 (ZIF8) decorated with polyacrylic acid. *RSC Adv.* 2021;11(16):9222-9234. doi: 10.1039/d0ra10423j
5. Wu W, Yu X, Sun J, *et al.* Zeolitic imidazolate framework (ZIF-8) decorated iron oxide nanoparticles loaded doxorubicin hydrochloride for osteosarcoma treatment - *in vitro* and *in vivo* preclinical studies. *Int J Nanomed.* 2023;18:7985-7999. doi: 10.2147/ijn.s438771
6. Iranpour S, Bahrami AR, Dayyani M, Saljooghi AS, Matin MM. A potent multifunctional ZIF-8 nanoplatform developed for colorectal cancer therapy by triple-delivery of chemo/radio/targeted therapy agents. *J Mater Chem B.* 2024;12(4):1096-1114. doi: 10.1039/d3tb02571c
7. Pan Y, Wang S, He X, *et al.* A combination of glioma *in vivo* imaging and *in vivo* drug delivery by metal-organic framework based composite nanoparticles. *J Mater Chem B.* 2019;7:7683-7689. doi: 10.1039/C9TB01651A
8. Huang J, Xu Z, Jiang Y, *et al.* Metal organic framework-coated gold nanorod as an on-demand drug delivery platform for chemo-photothermal cancer therapy. *J Nanobiotechnoloy.* 2021;19(1):219. doi: 10.1186/s12951-021-00961-x
9. Cravillon J, Munzer S, Lohmeier SJ, Feldhoff A, Huber K, Wiebcke M. Rapid room-temperature synthesis and characterization of nanocrystals of a prototypical zeolitic imidazolate framework. *Chem Mater.* 200;21:1410-1412. doi: 10.1021/cm900166h
10. Rajkumar K, Kanipandian N, Thirumurugan R. Toxicity assessment on haemotology, biochemical and histopathological alterations of silver nanoparticles-exposed freshwater fish. *Appl Nanosci.* 2016;6:19-29. doi: 10.1007/s13204-015-0417-7
11. Aravind SR, Joseph MM, Varghese S, Balaram P, Sreelekha TT. Antitumor and immunopotentiating activity of polysaccharide PST001 isolated from the seed kernel of Tamarindus indica: An *in vivo* study in mice. *ScientificWorldJournal.* 2012;2012:361382. doi: 10.1100/2012/361382
12. Joseph MM, Aravind SR, George SK, Pillai KR, Mini S, Sreelekha TT. Galactoxyloglucan-modified nanocarriers of doxorubicin for improved tumor-targeted drug delivery with minimal toxicity. *J Biomed Nanotechnol.* 2014;10(11):3253-3268. doi: 10.1166/jbn.2014.1957
13. Shimizu T, Kondo K, Hayaishi O. Role of prostaglandin endoperoxides in the serum thiobarbituric acid reaction. *Arch Biochem Biophys.* 1981;206(2):271-276. doi: 10.1016/0003-9861(81)90091-6
14. Axelrod B, Cheesbrough TM, Laasko S. Lipoxygenase from soybeans. *Methods Enzymol.* 1981;71:441-451. doi: 10.1016/0076-6879(81)71055-3
15. Bradley PP, Priebat DA, Christensen RD, Rothstein G. Measurement of cutaneous inflammation: Estimation of neutrophil content with an enzyme marker. *J Investig Dermatol.* 1982;78:206-209. doi: 10.1111/1523-1747.ep12506462
16. Salter M, Knowles RG. Assay of NOS activity by the measurement of conversion of oxyhemoglobin to methemoglobin by NO. *Methods Mol Biol.* 1998;100:61-65. doi: 10.1385/1-59259-749-1:61
17. Claiborne A. Catalase activity. In: Greenwald RA, editor. *CRC Handbook of Methods for Oxygen Radical Research.* Boca Raton: CRC Press; 1985. p. 283-284. doi: 10.1201/9781351072922.
18. Kakkar P, Das B, Viswanathan PN. A modified spectrophotometric assay of superoxide dismutase. *Indian J Biochem Biophys.* 1984;21(2):130-132.
19. Patterson JW, Lazarow A. Determination of glutathione. In: Glick D, editors. *Book Series: Methods of Biochemical Analysis.* Vol. 3. New York: Interscience; 1955. doi: 10.1002/9780470110188.ch9
20. Habig WH, Pabst MJ, Jakoby WB. Glutathione S-transferases. The first enzymatic step in mercapturic acid formation. *J Biol Chem.* 1974;249(22):7130-7139. doi: 10.1016/S0021-9258(19)42083-8
21. Mohandas J, Marshall JJ, Duggin GG, Horvath JS, Tiller DJ. Differential distribution of glutathione and glutathione-related enzymes in rabbit kidney. Possible implications in analgesic nephropathy. *Biochem Pharmacol.* 1984;33(11):1801-1807. doi: 10.1016/0006-2952(84)90353-8
22. Carlberg I, Mannervik B. Glutathione reductase. *Methods Enzymol.* 1985;113:484-490. doi: 10.1016/s0076-6879(85)13062-4
23. Buege JA, Aust SD. Microsomal lipid peroxidation. *Methods Enzymol.* 1978;52:302-310. doi: 10.1016/s0076-6879(78)52032-6

24. Lowry OH, Roseberough NJ, Farr AL, Randall RJ. Protein measurement with the Folin phenol reagent. *J Biol Chem.* 1951;193(1):265-275. doi: 10.1016/S0021-9258(19)52451-6
25. Awasthi KK, Verma R, Awasthi A, Awasthi K, Soni I, John PJ. *In vivo* genotoxic assessment of silver nanoparticles in liver cells of Swiss albino mice using comet assay. *Adv Mater Lett.* 2015;6:187-193. doi: 10.5185/amlett.2015.5640
26. Yang X, Schnackenberg LK, Shi Q, Salminen WF. Hepatic toxicity biomarkers. In: Gupta R, editors. *Biomarkers in Toxicology.* 2nd ed., Ch. 13. United States: Academic Press; 2014. p. 241-259. doi: 10.1016/b978-0-12-404630-6.00013-0
27. Thapa BR, Walia A. Liver function tests and their interpretation. *Indian J Pediatr.* 2007;74(7):663-671. doi: 10.1007/s12098-007-0118-7
28. Yao Y, Zang Y, Qu J, Tang M, Zhang T. The toxicity of metallic nanoparticles on liver: The subcellular damages, mechanisms, and outcomes. *Int J Nanomedicine.* 2019;14:8787-8804. doi: 10.2147/ijn.s212907
29. Bull H, Murray PG, Thomas D, Fraser AM, Nelson PN. Acid phosphatases. *Mol Pathol.* 2002;55(2):65-72. doi: 10.1136/mp.55.2.65
30. Fuchs TC, Hewitt P. Biomarkers for drug-induced renal damage and nephrotoxicity-an overview for applied toxicology. *AAPS J.* 2011;13(4):615-631. doi: 10.1208/s12248-011-9301-x
31. Giordano C, Karasik O, King-Morris K, Asmar A. Uric acid as a marker of kidney disease: Review of the current literature. *Dis Markers.* 2015;2015:382918. doi: 10.1155/2015/382918
32. Chen YC, Su CT, Wang ST, Lee HD, Lin SY. A preliminary investigation of the association between serum uric acid and impaired renal function. *Chang Gung Med J.* 2009;32(1):66-71.
33. Ramaiah L, Bounous DI, Elmore SA. *Hematopoietic System: Haschek and Rousseaux's Handbook of Toxicologic Pathology.* 3rd ed., Vol. 3., Ch. 50. Netherlands: Elsevier. p. 1863-1933; 2013. doi: 10.1016/b978-0-12-415759-0.00050-9
34. Braydich-Stolle L, Hussain S, Schlager JJ, Hofmann MC. *In vitro* cytotoxicity of nanoparticles in mammalian germline stem cells. *Toxicol Sci.* 2005;88(2):412-419. doi: 10.1093/toxsci/kfi256
35. Rosales C. Neutrophil: A cell with many roles in inflammation or several cell types? *Front Physiol.* 2018;9:113. doi: 10.3389/fphys.2018.00113
36. Liz R, Simard JC, Leonardi LB, Girard D. Silver nanoparticles rapidly induce atypical human neutrophil cell death by a process involving inflammatory caspases and reactive oxygen species and induce neutrophil extracellular traps release upon cell adhesion. *Int Immunopharmacol.* 2015;28(1):616-625. doi: 10.1016/j.intimp.2015.06.030
37. Bian Z, Guo Y, Ha B, Zen K, Liu Y. Regulation of the inflammatory response: Enhancing neutrophil infiltration under chronic inflammatory conditions. *J Immunol.* 2012;188(2):844-853. doi: 10.4049/jimmunol.1101736
38. Turini ME, DuBois RN. Cyclooxygenase-2: A therapeutic target. *Annu Rev Med.* 2002;53:35-57. doi: 10.1146/annurev.med.53.082901.103952
39. Seta F, Bachschmid M. *Cyclooxygenase Pathway of the Arachidonate Cascade.* South Asia: ELS; 2012. doi: 10.1002/9780470015902.a0023401
40. Dubois RN, Abramson SB, Crofford L, *et al.* Cyclooxygenase in biology and disease. *FASEB J.* 1998;12(12):1063-1073. doi: 10.1096/fasebj.12.12.1063
41. Gilbert NC, Rui Z, Neau DB, *et al.* Conversion of human 5-lipoxygenase to a 15-lipoxygenase by a point mutation to mimic phosphorylation at Serine-663. *FASEB J.* 2012;26(8):3222-3229. doi: 10.1096/fj.12-205286
42. Chandrasekharan JA, Sharma-Walia N. Lipoxins: Nature's way to resolve inflammation. *J Inflamm Res.* 2015;8:181-192. doi: 10.2147/JIR.S90380
43. Ndrepepa G. Myeloperoxidase - a bridge linking inflammation and oxidative stress with cardiovascular disease. *Clin Chim Acta.* 2019;493:36-51. doi: 10.1016/j.cca.2019.02.022
44. McSorley SJ, Liew FY. Nitric oxide. In: Delves PJ, editor. *Encyclopedia of Immunology.* 2nd ed; 1998. p. 1859-61.
45. Coleman JW. Nitric oxide in immunity and inflammation. *Int Immunopharmacol.* 2001;1(8):1397-1406. doi: 10.1016/s1567-5769(01)00086-8
46. Weydert CJ, Cullen JJ. Measurement of superoxide dismutase, catalase and glutathione peroxidase in cultured cells and tissue. *Nat Protoc.* 2010;5(1):51-66. doi: 10.1038/nprot.2009.197
47. Berg JM, Tymoczko J, Stryer L. *Biochemistry.* 5th ed. New York: W.H. Freeman; 2002.
48. Nandi A, Yan LJ, Jana CK, Das N. Role of catalase in oxidative stress- and age-associated degenerative diseases. *Oxid Med Cell Longev.* 2019;2019:9613090. doi: 10.1155/2019/9613090
49. Forman HJ, Zhang H, Rinna A. Glutathione: Overview of its protective roles, measurement, and biosynthesis. *Mol Aspects Med.* 2009;30(1-2):1-12. doi: 10.1016/j.mam.2008.08.006
50. Srinivas A, Rao PJ, Selvam G, Goparaju A, Murthy PB, Reddy PN. Oxidative stress and inflammatory responses of rat following acute inhalation exposure to iron oxide nanoparticles. *Hum Exp Toxicol.* 2012;31(11):1113-1131. doi: 10.1177/0960327112446515
51. Prabhakar PV, Reddy UA, Singh SP, *et al.* Oxidative stress induced by aluminum oxide nanomaterials after acute oral treatment in Wistar rats. *J Appl Toxicol.* 2012;32(6):436-445. doi: 10.1002/jat.1775. Retraction in: *J Appl Toxicol.* 2023;43(4):615. doi: 10.1002/jat.4412
52. Moron MS, Depierre JW, Mannervik B. Levels of glutathione, glutathione reductase and glutathione S-transferase activities in rat lung and liver. *Biochim Biophys Acta.* 1979;582(1):67-78. doi: 10.1016/0304-4165(79)90289-7
53. Gawel S, Wardas M, Niedworok E, Wardas P. Malondialdehyde (MDA) as a lipid peroxidation marker. *Wiad Lek.* 2004;57(9-10):453-455.
54. Ito F, Sono Y, Ito T. Measurement and clinical significance of lipid peroxidation as a biomarker of oxidative stress: Oxidative stress in diabetes, atherosclerosis, and chronic inflammation. *Antioxidants (Basel).* 2019;8(3):72. doi: 10.3390/antiox8030072
55. Birben E, Sahiner UM, Sackesen C, Erzurum S, Kalayci O. Oxidative stress and antioxidant defense. *World Allergy Organ J.* 2012;5(1):9-19. doi: 10.1097/wox.0b013e3182439613
56. Manke A, Wang L, Rojanasakul Y. Mechanisms of nanoparticle-induced oxidative stress and toxicity. *Biomed Res Int.* 2013;2013:942916. doi: 10.1155/2013/942916
57. Vergani L, Floreani M, Russell A, *et al.* Antioxidant defences and homeostasis of reactive oxygen species in different human mitochondrial DNA-depleted cell lines. *Eur J Biochem.* 2004;271(18):3646-3656. doi: 10.1111/j.1432-1033.2004.04298.x
58. Haque R, Bin-Hafeez B, Parvez S, *et al.* Aqueous extract of walnut (*Juglans regia* L.) protects mice against cyclophosphamide-induced biochemical toxicity. *Hum Exp Toxicol.* 2003;22(9):473-480. doi: 10.1191/0960327103ht388oa
59. Elsabahy M, Wooley KL. Cytokines as biomarkers of nanoparticle immunotoxicity. *Chem Soc Rev.* 2013;42(12):5552-5576. doi: 10.1039/c3cs60064e
60. Ibrahim KE, Al-Mutary MG, Bakhiet AO, Khan HA. Histopathology of the liver, kidney, and spleen of mice exposed to gold nanoparticles. *Molecules.* 2018;23(8):1848. doi: 10.3390/molecules23081848
61. Awaad A. Histopathological and immunological changes induced by magnetite nanoparticles in the spleen, liver and genital tract of mice following intravaginal instillation. *J Basic Appl Zool.* 2015;71:32-47. doi: 10.1016/j.jobaz.2015.03.003
62. Ajdari M, Ghahnavieh MZ. Histopathology effects of nickel nanoparticles on lungs, liver, and spleen tissues in male mice. *Int Nano Lett.* 2014;4:113. doi: 10.1007/s40089-014-0113-8
63. Wu A, Han M, Ni Z, *et al.* Multifunctional Sr/Se co-doped ZIF-8

nanozyme for chemo/chemodynamic synergistic tumor therapy via apoptosis and ferroptosis. *Theranostics*. 2024;14(5):1939-1955. doi: 10.7150/thno.92663

64. Gong L, Zhao H, Chen L, Liu Y, *et al*. Novel peptide-modified zeolitic imidazolate framework-8 nanoparticles with pH-sensitive release of doxorubicin for targeted treatment of colorectal cancer. Pharmaceutics. 2025;17(2):246. doi: 10.3390/pharmaceutics17020246
65. Mao Y, Wang L, Xu Z, *et al*. Developing a selection framework for zinc ion-based biomaterial design: Guided by the biosafety assessment of ZIF-8 and ZnO. *ACS Biomater Sci Eng*. 2024;10(5):2967-2982. doi: 10.1021/acsbiomaterials.3c01693
66. Kumari S, Howlett TS, Ehrman RN, *et al*. *In vivo* biocompatibility of ZIF-8 for slow release via intranasal administration. *Chem Sci*. 2023;14(21):5774-5782. doi: 10.1039/d3sc00500c

Received: May 31, 2025
1st revised: May 26, 2025
2nd revised: August 4, 2025
Accepted: August 5, 2025
Available online: September 10, 2025